



Title	Magnetostratigraphic dating of the prime-time sedimentary record of Himalayan tectonics and climate: new age constraints (13-10 Ma) from the Siwaliks of the Tinau Khola north section, Nepal
Author(s)	Gautam, Pitambar; Ulak, Prakash Das; Paudyal, Khum Narayan; Gyawali, Babu Ram; Bhandari, Sudarshan
Citation	Geophysical Journal International, 190, 1378-1392 https://doi.org/10.1111/j.1365-246X.2012.05568.x
Issue Date	2012-06
Doc URL	http://hdl.handle.net/2115/50012
Type	article
File Information	j.1365-246X.2012.05568.x.pdf



[Instructions for use](#)

Magnetostratigraphic dating of the prime-time sedimentary record of Himalayan tectonics and climate: new age constraints (13–10 Ma) from the Siwaliks of the Tinau Khola north section, Nepal

Pitambar Gautam,^{1,*} Prakash Das Ulak,² Khum Narayan Paudyal,³ Babu Ram Gyawali³ and Sudarshan Bhandari³

¹Creative Research Institution (CRIS), Hokkaido University, N21, W10, Kita-ku, Hokkaido 001–0021, Sapporo, Japan. E-mail: pgautam@cris.hokudai.ac.jp

²Department of Geology, Trichandra Camus, Tribhuvan University, Kathmandu, Nepal

³Central Department of Geology, Tribhuvan University, Kirtipur, Kathmandu, Nepal

Accepted 2012 June 5. Received 2012 June 1; in original form 2011 December 29

SUMMARY

A molasse sequence comprising 1.5-km-thick sediments of the Lower and Middle Siwaliks Group in the sub-Himalayan North Belt along the Tinau Khola River in west-central Nepal was studied for the low-field magnetic susceptibility and anisotropy using single core specimens of siltstone/sandstone from 127 stratigraphic levels. The magnetic fabric comprises primary sedimentary-compactional and secondary tectonic components. It is characterized by (i) predominantly oblate magnetic susceptibility anisotropy ellipsoids, (ii) low anisotropy (P' mostly <1.1) and low magnetic susceptibility ($<ca. 10^{-7} \text{ m}^3 \text{ kg}^{-1}$) contributed mainly by paramagnetic and diamagnetic minerals and (iii) WNW–ESE magnetic lineations subparallel to the fold axes/bedding strikes/thrust front, and hence normal to the direction of palaeotectonic compression.

Thermal demagnetization of single core specimens from 103 levels across 1120 m of the lower part revealed a characteristic remanence of the high unblocking temperature ($> 600 \text{ }^\circ\text{C}$) in hematite. Remanence ratios derived from demagnetization data allowed the first-order estimation of remanence contributions from magnetic minerals (goethite, maghemite, magnetite and hematite), and discrimination of rockmagnetic zones correlatable with distinct lithofacies, which will facilitate objective mapping. We correlated a magnetic polarity sequence, constructed from normal and reverse polarity directions from 77 levels that passed the reversal test and represented primary remanences, with the standard geomagnetic polarity timescale to constrain the depositional age between *ca.* 13.2 Ma (base of Chron C5AAN, 13.015–13.183 Ma) and the middle of Chron C5n.2n (9.987–11.040 Ma). We calculated the sediment accumulation rate for polarity zones from the chronologically better constrained part below Chron C5n.2n (i.e. below 11.040 Ma) to be 25–61 cm kyr^{-1} (average, 39 cm kyr^{-1}), which is consistent with the value of 32–50 cm kyr^{-1} reported from Siwaik sections in Nepal. The notable increase in accumulation rate after 12.1 Ma probably reflects the peak of the earlier phase of uplift and/or unroofing of the Himalayan source region followed by rapid accumulation in the fore-deep, and a link to monsoon initiation/intensification. Compared to the expected remanence from the latest APWP for the Indian Plate 10–13 Ma, the best-defined mean ($351.8^\circ/20.9^\circ$) is rotated anticlockwise by 9.2° and records an inclination shallowing of 25° . Constraining the base of the Tinau Khola north section to 13.2 Ma (i.e. older than the Tinau Khola south by 1.7 Myr) should open up new horizons for multidisciplinary and multiproxy research targeting geotectonic/climatic/environmental palaeoreconstructions of Himalaya-wide events.

Key words: Magnetic fabrics and anisotropy; Magnetostratigraphy; Rock and mineral magnetism; Asia.

*Also at: The Hokkaido University Museum, Hokkaido University, N10, W8, Kita-ku, Hokkaido 060–0810, Sapporo, Japan

INTRODUCTION

The Siwalik or Churia Group is composed of Mio-Pliocene fluvial foreland basin sediments (FBS) occurring in the sub-Himalayan fold-and-thrust belt (FTB) along the southern margin of the Himalayan mountain arc. This group represents an important sediment archive of the chronology and mechanisms of past palaeoclimatic (e.g. initiation of monsoon and its fluctuations), tectonosedimentary (complex interplays between uplift, weathering, erosion, transportation, deposition, etc.) and biotic events in the Himalaya and adjacent regions (e.g. Flynn *et al.* 1990; Opdyke 1990; Tokuoka *et al.* 1990; Mugnier *et al.* 1993; Dhital *et al.* 1995; Burbank *et al.* 1996; Gautam & Rösler 1999; Nakayama & Ulak 1999; Molnar 2005; Huyghe *et al.* 2005). The Nepalese FBSs lack fossils for reasonably accurate dating (e.g. with precision of *ca.* 1 Myr or less) and lack radioisotopically datable material (e.g. volcanic ash, etc.) suitable for determining depositional ages. Thermochronometry based on detrital zircon and apatite grains has increasingly been used to determine source-area exhumation dates and thence to constrain the maximum possible depositional ages of these sediments in the foredeep that constitutes the present-day sub-Himalaya (West *et al.* 1991; Beek *et al.* 2006; Bernet *et al.* 2006; Szulc *et al.* 2006). Magnetostratigraphic dating conducted successfully over the past three decades has largely overcome this problem, not only by constraining the chronology of sediment deposition in the sub-Himalaya itself but also in deciphering the timing of tectonic and climatic phenomena in the central part of the Himalayan Range (Tokuoka *et al.* 1986; Appel *et al.* 1991; Harrison *et al.* 1993; Gautam & Appel 1994; Tanaka 1997; Rösler *et al.* 1997; Rösler & Appel 1998; Gautam & Rösler 1999; Gautam & Fujiwara 2000; Ojha *et al.* 2000).

Anisotropy of magnetic susceptibility (AMS) measurements have been made in the FBSs along the FTB to establish the sedimentary and/or tectonic nature of the magnetic fabric (e.g. Tauxe *et al.* 1990; Gautam & Rösler 1999; Robion *et al.* 2007). The magnetic fabric contributed mainly by paramagnetic and diamagnetic minerals exhibits weak anisotropy, an oblate shape of the AMS ellipsoids and the clustering of the minimum AMS axes on the pole to bedding, suggesting compaction as the predominant influence. Furthermore, the magnetic lineation defined by the maximum AMS axes is closely parallel to the fold-and-thrust axes, and hence perpendicular to the direction of syn-sedimentary compression active throughout the foredeep, as has been found in compressive settings in the external Apennines in Italy and the coastal range of Taiwan (Lee *et al.* 1990; Sagnotti *et al.* 1998; Gautam *et al.* 2000). In an attempt to elucidate the spatiotemporal variation in compression direction estimated under the assumption of orthogonality to the mean magnetic lineation, Gautam (2008) reviewed magnetostratigraphic age constraints and the AMS data for five different sections in the Nepalese sector of the sub-Himalayan zone.

This study was part of our ongoing studies of magnetostratigraphy and magnetic fabric in the Nepalese sub-Himalaya. Its aim was to gather high-resolution magnetic polarity data for accurate determination of the depositional ages of the FBSs; for better dating of tectonic, climatic (e.g. Asian monsoon initiation and its intensification periods) and biotic events; and for devising proxies (e.g. pre-folding tectonic magnetic lineations) for reconstructing the palaeocompression direction in the Himalayas (Gautam & Rösler 1999; Gautam 2008). The study targeted the Churia (Siwalik) Group sediments in the Tinau Khola north section (Tinau-N) in the sub-Himalayan North Belt (Tokuoka *et al.* 1990), and relied on the results of a similar study of the Tinau Khola south section (Tinau-

S) comprising the lithologies of the Lower and Middle Siwaliks in the South Belt (Gautam & Appel 1994; Figs 1a and b). Recalibration (Gautam & Rösler 1999) of the Tinau-S magnetic polarity sequence (MPS) with geomagnetic polarity timescale (GPTS) CK95 (Cande & Kent 1995) revealed: (i) a depositional age of 11.5–5.9 Ma for a 1710-m section; (ii) an age of 9.31 Ma for the *Sivapithecus punjabicus* horizon (Munthe *et al.* 1983) near the top of the Arung Khola Upper Member; and (iii) a sediment accumulation rate (SAR) of 29–37 cm kyr⁻¹ (non-linear with time; average 32 cm kyr⁻¹; rates commonly higher for sandstone-dominated sections). Justification for the new study included the availability of sediments much older than those in Tinau-S, as shown by detailed mapping (Tokuoka *et al.* 1990; Ulak & Nakayama 2001); easy accessibility of the site; and the renewed importance of precise chronology of sediments of >10 Ma for interpreting multidisciplinary proxies for past climatic/tectonic events in the Himalaya.

GEOLOGY AND SAMPLING

Siwalik Group sediments derived from the erosion of the main Himalayan Range, which underwent episodic uplifts following the India–Eurasia collision in the Early Tertiary. The sub-Himalayan FTB package that has preserved these sediments in west-central Nepal north of Butwal is composed of two belts (South Belt, <5 km wide; North Belt, <2.5 km wide) separated by the Intra-Siwalik Thrust, locally called the Central Churia Thrust (CCT; Tokuoka *et al.* 1986). The CCT strikes almost E–W, is subvertical at the surface and passes just north of the confluence of Tinau Khola and Jhumsa Khola in the study area. The North belt in this area comprises the Arung Khola Formation and Binai Khola Formation; the former covers the Lower Siwaliks and part of the Middle Siwaliks, whereas the latter encompasses the rest of Middle Siwaliks (Fig. 1).

The age of Nepalese Siwalik sediments deposited at a rate of *ca.* 40 cm kyr⁻¹ can reasonably be determined through magnetostratigraphic correlation achieved by sampling a section at least 1000-m thick at a sampling density of at least once every 30 m, enough to ensure that 3 points fall within a distinct polarity zone (thickness, 100 m; duration, 0.25 Myr; Gautam & Rösler 1999). In consideration of variation in lithology and associated SARs along the section, difficulty in measuring characteristic remanent magnetization (ChRM) in specimens heavily overprinted by secondary remanences, and for extracting rockmagnetic parameters to aid in mapping lithofacies, our sampling strategy favoured drilling with denser and non-uniform spacing along the stratigraphic column.

During sampling, we also prepared lithological columns. Ten samples (1–10) were taken just north of the confluence of the Tinau and Jhumsa rivers (Fig. 1), along an exposure *ca.* 10-m thick, consisting of alternating layers of light grey and reddish grey fine sandstone and thinly laminated dark grey mudstone, with the occasional occurrence of pebbly sandstones containing mudclasts or concretions. These sediments strongly resemble in lithology with the Middle Siwaliks and hence constitute the top of the South Belt. The strata there dip 60–75° NNE. Towards north, there follows *ca.* 85-m long gap sheared talus-covered or vegetated zone devoid of *in situ* outcrops marked by the CCT.

A detailed lithology was constructed along the banks of the Tinau Khola upstream from the Jhumsa–Tinau confluence, first along the river (up to level 99) and then along the roadside (levels 100–137) on the route (Fig. 1b). Sampling level 11 was the

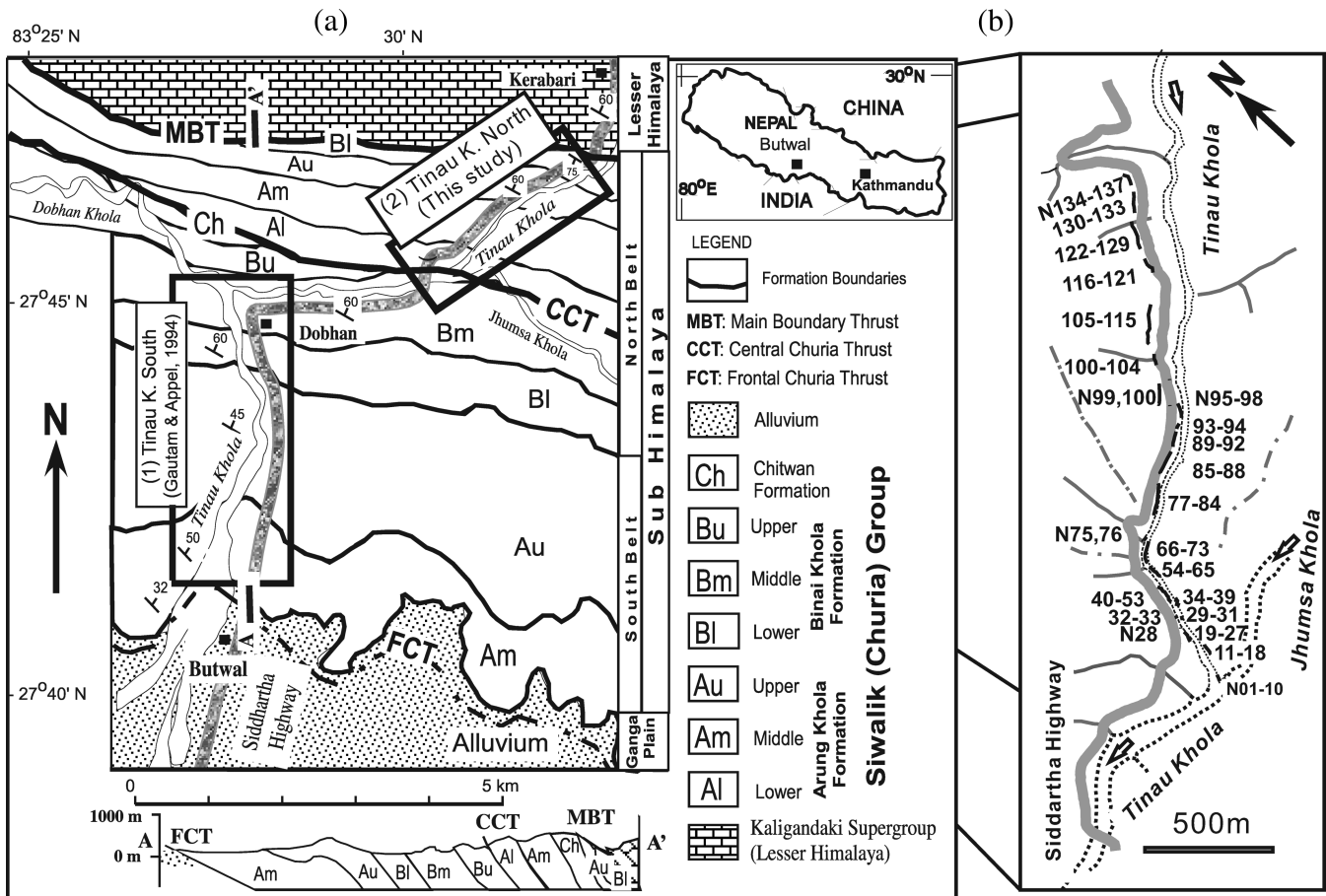


Figure 1. (a) Geological sketch map of Tinau Khola area near Butwal, west-central Nepal (modified from Ulak & Nakayama 2001). The sub-Himalayan zone, separated from the alluvial Ganga Plain to the south by the Frontal Churia Thrust (FCT) and the Lesser Himalaya to the north by the Main Boundary Thrust (MBT), comprises the Siwalik (Churia) Group sediments. The Siwaliks occur in the North and South Belts subdivided by the Central Churia Thrust (CCT) running approximately WNW–ESE. The two rectangular areas labelled ‘(1) Tinau K. south’ and ‘(2) Tinau K. north’ mark the section of Gautam & Appel (1994) and the new section in this study, respectively. (b) Enlarged view of area (2) showing the Tinau Khola river course and the trace of Siddhartha Highway and indicating sediment core drilling levels (N1–N99, riverbanks; N100–N137, roadside). Drilling levels N1–N10, located on the left bank of the Tinau Khola near its confluence with Jhumsa Khola, lie south of the CCT zone and therefore belong to the South Belt (for details, refer to text). The magnetic fabric study covered a thickness of 1450 m, whereas the magnetic polarity and rockmagnetic zonation were restricted to the lower part, 1120-m thick (samples N11–N116).

first outcrop comprising layers of mudstone (ms), often variegated and with concretions, alternating with subordinate fine-grained sandstones (ss), commonly grey, with the ripple laminations and concretions typical of the Lower Siwaliks, corresponding to the lower member of the Arung Khola Formation (Al; ms > ss and ms variegated). Most of the first 200-m-thick section exhibits slightly overturned to subvertical bedding (southerly dips of ca. 70–90°). The riverbank further upstream exposes another 750-m-thick section with consistent northerly dips of ca. 80°, after which the steep river gorge is not suitable for sampling because of either inaccessibility or large gaps in sediment outcrops. For this reason, sampling was shifted to the road-cut exposure just above the right bank along the Siddhartha Highway to cover another 500-m section with variable northerly dips of 60–80°. Representative logs selected to show variation along the section are presented in Fig. 2. The Al/Am boundary marking the appearance of less-variegated ms occurring in equal amounts to ss is evident between levels 69 and 70. The Am/Au boundary marking the beginning of the occurrence of salt-and-pepper sandstones is evident just above level 107.

Each sampling level for magnetic study typically comprised up to three cores (2.54 cm in diameter and up to 10 cm long) made

with a drill powered by a commercial portable gasoline engine. Cores were taken from indurated mudstone, siltstone, and sandstone (fine grained, whenever possible) beds known to have accessible yet consistent ChRM suitable for magnetostratigraphy (e.g. Tauxe & Badgley 1988; Friedman *et al.* 1992; Gautam & Rösler 1999). Sampling levels 1–99 were located along the riverbank (either left or right, dictated by accessibility) upstream from the river junction (27°32.69′N, 83°50.22′E). Owing to inaccessibility immediately upstream from level 99 and lack of river exposures thereafter, further sampling (levels 100–137) was continued along the road wall between (27°45.41′N, 83°30.77′E) and the big bend of the road at (27°45.78′N, 83°31.12′E) until the sediments became too coarse and highly weathered.

LABORATORY PROCEDURES

Several standard specimens of ca. 2.2-cm length were cut from the cores in the laboratory for measurements of natural remanent magnetization (NRM), magnetic susceptibility (MS), and isothermal remanent magnetization (IRM). Instruments employed

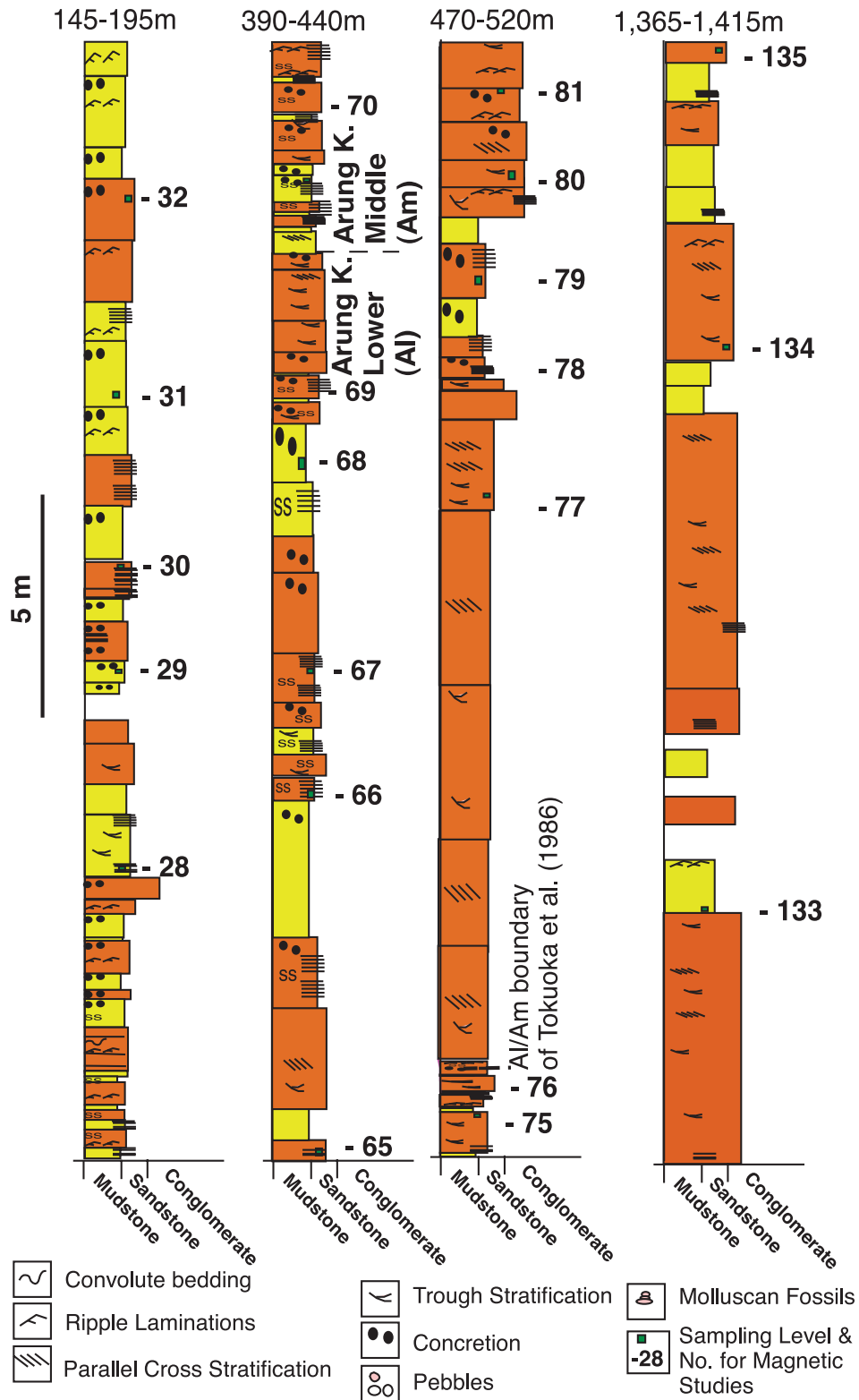


Figure 2. Lithological columns for the Tinau Khola north section, showing variation in lithology and sedimentary style up-section. Each column covers a 50-m interval. We relocated the Al/Am boundary to 427 m (from CCT), about 50 m below the level proposed by Tokuoka *et al.* (1986). The section at the right is typical for Middle Siwalik lithologies, corresponding here mainly to the Au or partly to the Binai Khola Lower Member.

included a 755R SQUID (2G Enterprises, Sand City, CA, USA) magnetometer for measurement of remanence; a Schoenstedt furnace for progressive thermal demagnetization (ThD); a KLY-2,3 (AGICO, Brno, Czech Republic) kappabridge for measuring low-

field MS and its anisotropy; a MMPM9 (Magnetic Measurements, Aughton, Lancs, UK) pulse magnetizer with 2.5 T capacity to impart IRM to a few specimens; and a fluxgate spinner magnetometer (Molspin Limited, Newcastle On Tyne, UK) to measure the IRM

acquired after each step of magnetization acquisition. Measurements were carried out mostly at the palaeomagnetic laboratory of the University of Tübingen. AMS was also measured at the Kochi Core Center, Kochi University. Progressive ThD to extract magnetization components was limited to one specimen from each sampling level, as this practice is adequate for obtaining details of the MPS from Nepalese sections sampled at close spacing (*ca.* 10 m; see Gautam & Fujiwara 2000 and references therein). The ThD data were analysed using the Munich University PALMAG program, which can perform principal component analysis (PCA; Kirschvink 1980) and field tests for palaeomagnetic stability. Additional details about the equipment used, ThD procedure, and data acquisition and processing techniques for remanence as well as anisotropy are given in Gautam & Appel (1994) and Gautam *et al.* (2000).

MAGNETIC MEASUREMENTS: RESULTS AND DISCUSSION

Magnetomineralogy, demagnetization behavior and rockmagnetic zonation

Magnetic mineralogy from IRM acquisition

Details on the magnetic properties of the Siwalik sediments from Nepal are well known from joint analyses of IRM acquisition curves and unblocking temperature ranges of IRM, as well as by NRM (Gautam & Rösler 1999 and references therein; Gautam *et al.* 2000; Gautam & Fujiwara 2000). The magnetomineralogical interpretation of the Tinau-N section was based on a coercivity spectrum analysis of the IRM data, newly acquired for a few specimens, following the log-normal Gaussian decomposition technique, to discriminate the contribution of magnetic mineral phases with differing coercivity spectra, as outlined by Kruijer *et al.* (2001). We tested the validity of this new approach for the Nepalese Siwalik sediments by performing a parallel analysis on IRM data from Karnali-section specimens for which the magnetic minerals were known from the ThD behaviour of IRM and NRM (for goethite and hematite) and from Curie temperature data (for maghemite and magnetite), as discussed in Gautam *et al.* (2000).

IRM acquisition curves and modelling data for four specimens from Karnali and Tinau-N sections are presented in Fig. 3 and Table 1. The data indicate up to five components with distinct median acquisition fields ($B_{1/2}$), that is, Comp1 (*ca.* 30 mT), Comp2 (70 mT), Comp3 (140–250 mT) and Comp4 (550–660 mT), Comp5 (>1500 mT). The logarithmic dispersion parameter (defined as the half-width of the gradient curve corresponding to a logarithmic Gaussian distribution curve at the level of one standard deviation from $B_{1/2}$) is broad (0.33–0.35) for Comp1, whereas for others it ranges from 0.18 to 0.25. In view of the magnetomineralogical interpretation for the Karnali specimens partially shown by the dominant IRM ThD ranges in Table 1 and other data from the literature for Siwalik sediments, Comp1, Comp4 and Comp5 are related to magnetite (soft coercivity), hematite (hard coercivity) and goethite (very hard coercivity), respectively (Peters & Dekkers 2003; Gautam *et al.* 2005b). We infer Comp3 of intermediate coercivity found in all specimens in substantial quantities to be maghemite, judging from the notable decrease in magnetic remanence by 400 °C during demagnetization. However, an alternative interpretation of Comp3 as ‘soft hematite’ is also plausible because of the very wide coercivity range (28–769 mT) assigned to hematite in the published literature (Peters & Dekkers 2003; Fig. 3; Table 1). This mineral phase, which

can have unblocking temperatures as low as 300 °C, has been suspected in sediments from the Nepalese Siwaliks (Rösler & Appel 1998; Gautam *et al.* 2005a). We also suspect that Comp2 observed in specimen N106b, which was relatively highly weathered, is also a maghemite-like phase. In the Siwalik sediments, specimens such as N58a (IRM contribution: 24.3 per cent) that contain abundant high-coercivity or hard hematite are suitable for recovering ChRM, whereas those like N106b, with a low (<10 per cent) contribution to IRM from high-coercivity hematite and a very high proportion of intermediate- and low-coercivity phases known to carry a recent field (RF) overprint, are less suitable (Gautam & Rösler 1999).

Demagnetization behaviour

To recover ChRM residing in hard-coercivity hematite, at least one specimen cut from an independently oriented core drilled from each distinct stratigraphic level was subjected to stepwise ThD in progressively higher temperature steps (commonly at 150, 400, 500, 565, 600, 640 and 665 °C). Remanence measurements were limited to 103 levels from the lower 1120 m section. The reason for this was the suspected presence of additional maghemite, derived from weathering-induced low-temperature oxidation in the relatively high MS samples from most roadside outcrops, and prone to conversion to magnetite upon ThD at high temperatures. This would lead to laboratory-induced noise and make the isolation of hematite-based ChRM difficult.

Fig. 4 presents the results of demagnetization of three representative specimens. The demagnetization paths indicate two components: a low- to moderate-unblocking temperature component commonly demagnetized by 150 °C or 40 °C (all three specimens in Fig. 4), and a high-unblocking temperature component surviving up to well above 600 °C (specimens N58b and N43b). At the sampling locality, the former component (with a northerly declination and moderately downward inclination) was parallel to the present-day field ($I = 47^\circ$), and we interpret the magnetization as secondary, representing the RF. The RF component can be attributed to goethite, maghemite, magnetite or even pigmentary hematite, depending on the maximum unblocking temperature or the ranges within which differing fractions of the total remanence were demagnetized (e.g. Gautam & Appel 1994; Rösler & Appel 1998). In contrast, the high-temperature component had either a westerly declination and a moderate to steep downward inclination or an easterly declination and a moderate to steep upward inclination. It clearly differed from the present-day field, and the bedding-tilt correction yielded northerly (shallow downward) or southerly (shallow upward) directions that resemble the dual-polarity ChRM in Siwalik sediments from numerous sections in Nepal, India and Pakistan. Hence, we considered this component to be the ChRM. Past demagnetization studies and laboratory experiments have demonstrated that a ChRM with unblocking temperatures exceeding 600 °C, and in which a significant portion of remanence is demagnetized in a very high temperature range (e.g. 640–680 °C), is a primary detrital remanence carried by specular hematite, whereas the remanence unblocked below 600 °C may represent a secondary remanence carried by pigmentary hematite (e.g. a chemical remanence resembling the primary ChRM, but unblocked in the 525–600 °C range, in the Pakistani Middle Siwaliks) or ‘soft hematite’ (a label assigned to secondary remanence unblocked within the wide temperature range of 300–625 °C in the Siwaliks in the Surai Khola section; Tauxe *et al.* 1980; Butler 1992: p. 176; Rösler & Appel 1998). Specimen N106a shows exceptional behaviour because the

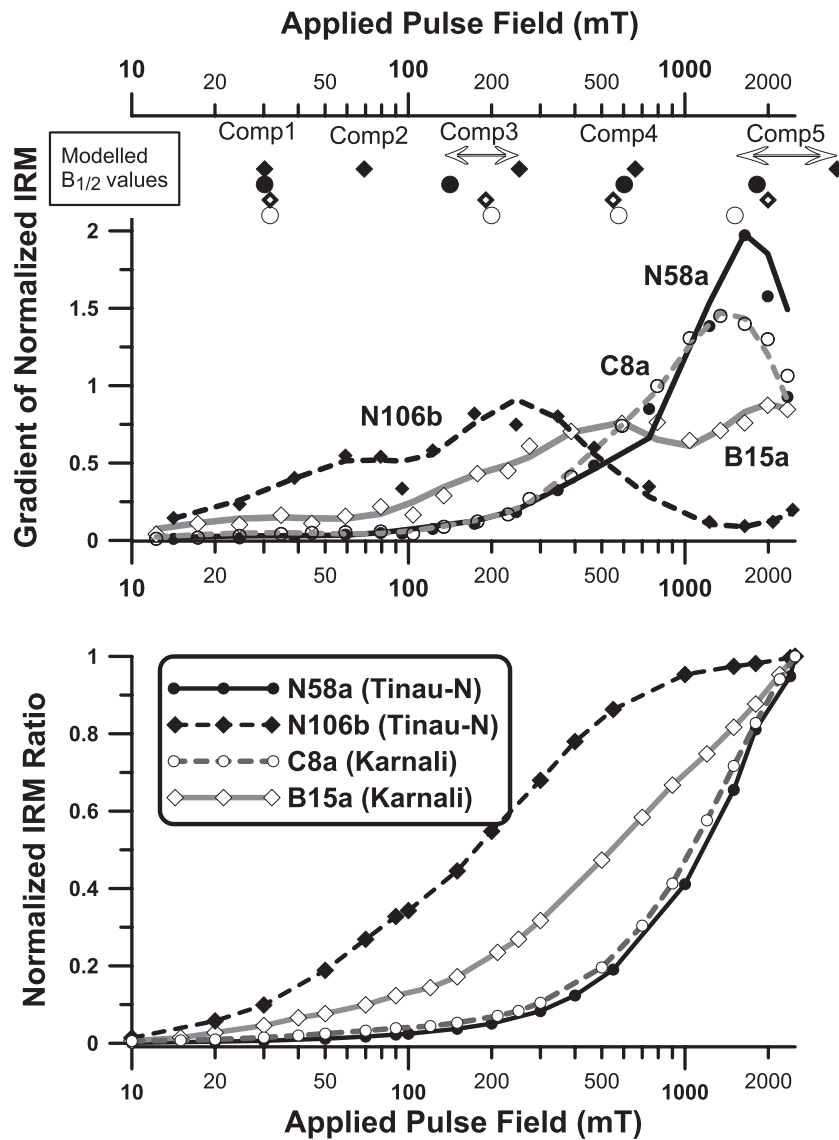


Figure 3. (a) Normalized isothermal remanent magnetization (IRM) acquisition curves for four specimens, two each from the Karnali section and Tinau Khola north section. The shape of each curve was determined by the number of remanence-carrying minerals, each with a characteristic rate of acquisition and saturation behavior. (b) IRM gradient data (discrete symbols) derived from the normalized IRM curves and modelled curves fitting the respective gradient data (continuous lines). The curves were obtained by summing the gradients for all components, each of which had a distinct relative magnitude, median acquisition field ($B_{1/2}$) and logarithmic dispersion parameter (DP) resulting from a coercivity spectrum analysis as described by Kruijer *et al.* (2001). In the modelled curves, the abscissa value of each maximum peak roughly corresponds to $B_{1/2}$ of the corresponding component, indicated by different symbols for each specimen in (c). Each curve reasonably well fits three–five components, whose parameters are given in Table 1. The inferred prominent minerals (approximate $B_{1/2}$) are magnetite (*ca.* 30 mT), maghemite? or ‘soft hematite’? (140–250 mT), hematite (550–660 mT) and goethite (>1500 mT).

RF component is the sole direction surviving up to very high temperatures.

Rockmagnetic zonation

Fig. 5 shows variation with stratigraphic height in the MS, NRM intensity and relative remanence contributions of various minerals. Our basic assumption was that the ratios of NRM magnitudes demagnetized below 150 °C, from 150 °C to 400 °C, from 400 °C to 600 °C and above 600 °C to the initial NRM provided first-order estimates of the remanence contributions by goethite (αFeOOH), maghemite ($\gamma\text{Fe}_2\text{O}_3$), magnetite (Fe_3O_4) and hematite ($\alpha\text{Fe}_2\text{O}_3$), respectively, because these temperature steps are higher than the

Curie Neel or decomposition temperatures of the respective minerals (Dunlop & Özdemir 1997; Gautam & Fujiwara 2000).

The mass-specific MS (in $10^{-8} \text{ m}^3 \text{ kg}^{-1}$) ranged mostly between 2 and 10, whereas the NRM intensity (in m Am^{-1}) varied between 0.1 and 10. MS fluctuated more frequently than the other parameters (NRM and the ratios), without clear correlations to the latter. A significant positive MS step occurred above level 106, close to the Am/Au boundary at level 107 based on changes in lithofacies, coinciding with elevated contributions from ‘magnetite’ and ‘maghemite’. Judging from the ratios as contributors of various minerals, a notable increase occurred at around level 37, where an outcrop-scale lithological change occurred, from thickly bedded grey sandstones intercalated with mudstones to medium-bedded reddish brown sandy beds alternating with similarly thick

Table 1. Magnetomineralogy based on a coercivity spectrum analysis of data on isothermal remanent magnetization (IRM) acquisition and demagnetization.

Specimen	Component	Contribution	$\log(B/2)$	$B/2$	DP	Magnetic mineral inferred	Inferred dominant IRM thermal demagnetization range ($^{\circ}\text{C}$) ^a
		Per cent	mT	mT	mT		
1. Karnali River section (^a IRM acquisition and demagnetization data after Gautam <i>et al.</i> 2000)							
C8a	Comp1	3.8	1.50	31.6	0.33	Magnetite	400–600
	Comp3	5.5	2.30	199.5	0.22	Maghemite or 'soft' hematite?	200–400
	Comp4	25.7	2.76	575.4	0.20	Hematite	620–675
	Comp5	65.0	3.18	1513.6	0.20	Goethite	Up to 100
	B15a	Comp1	10.6	1.50	31.6	0.35	Magnetite
	Comp3	17.7	2.28	190.5	0.20	Maghemite or 'soft' hematite?	200–360
	Comp4	33.6	2.74	549.5	0.21	Hematite	600–675
	Comp5	38.1	3.30	1995.3	0.20	Goethite	Up to 150
2. Tinau Khola north section							
N58a	Comp1	2.1	1.48	30.2	0.34	Magnetite	Data not available
	Comp3	3.2	2.15	141.3	0.20	Maghemite or 'soft hematite'?	
	Comp4	24.3	2.78	602.6	0.25	Hematite	
	Comp5	70.4	3.26	1819.7	0.18	Goethite	
	N106b	Comp1	17.4	1.48	30.2	0.34	Magnetite
	Comp2	18.3	1.84	69.2	0.22	Maghemite?	
	Comp3	44.0	2.40	251.2	0.22	Maghemite or 'soft' hematite?	
	Comp4	9.2	2.82	660.7	0.20	Hematite	
	Comp5	11.0	3.55	3548.1	0.20	Goethite	

Note: Component data derived from joint analyses of IRM acquisition and gradient plots shown in Fig. 3 following Kruijer *et al.* (2001). The IRM gradient curve is the sum of lognormal distribution curves of a number of components, each being uniquely defined by the mean remanence coercivity [$\log(B/2)$] and the logarithmic dispersion parameter (DP).

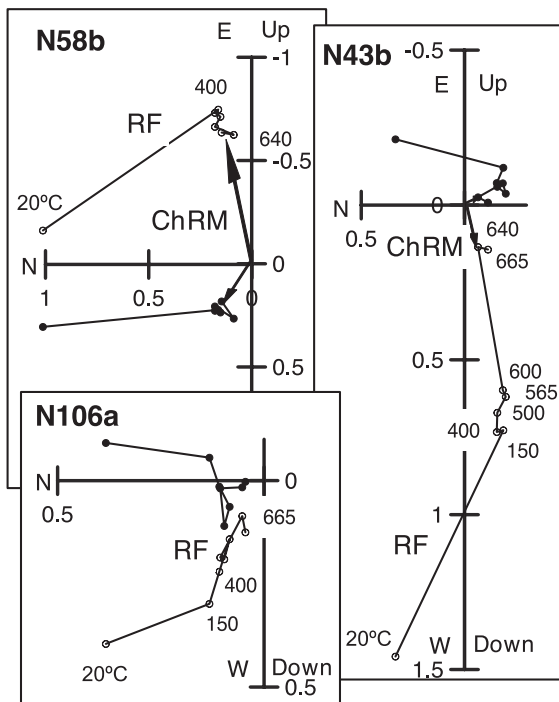


Figure 4. Orthogonal Zijderveld-type vector plots showing the thermal demagnetization behaviour of representative specimens from levels 58, 43 and 106. The *in situ* remanence direction at each demagnetization temperature ($^{\circ}\text{C}$) is represented by a pair of projections from the remanent magnetization vector in the NS–EW horizontal plane (solid circles) and NS–Up/Down vertical plane (open circles), respectively. RF, recent field component, residing in goethite, maghemite or even magnetite; ChRM, characteristic remanence carried by hematite. The unit of remanence magnitude along the horizontal and vertical axes is m Am^{-1} .

mudstones. Another shift in these ratios at around level 100 is likely an artefact related to the increased amount of magnetic minerals produced by low-temperature oxidation in the roadside outcrops, which are prone to more weathering than the outcrops in the river section below. The combined plots allow discrimination of the five rockmagnetic zones (RMZs) shown at the extreme right of Fig. 5. Remarkably, the Al/Am and Am/Au boundaries coincide with the III–IV and IV–V transitions in the RMZs. These tentative observations suggest that the rock magnetic zonation is a tool that can potentially aid geological mapping in the sub-Himalaya, especially at the level of stratigraphic members or lithofacies.

Chronological, sedimentary, and tectonic implications of the magnetic polarity stratigraphy

Isolation of magnetization components constituting NRM

We estimated the RF component demagnetized mostly below 400°C step using three data points estimated by PCA (NRM, 150°C and 400°C), without anchoring in specimens from 100 levels. The mean direction had a northerly declination and moderate inclination ($I = 51^{\circ}$), confirming that it represents the present-day field direction ($D = 0^{\circ}$, $I = 47^{\circ}$) at the sampling locality (28.51°N , 83.75°E).

We employed the 'anchored' line-fitting option in PCA to calculate the ChRM directions for 102 levels, using demagnetization data above 600°C , but further considered only 86 levels with a maximum angular deviation (MAD) $\leq 15^{\circ}$ (Fig. 6a). After corrections for bedding tilt (Fig. 6b), these directions converged into two roughly antipodal clusters (Fig. 6c) represented by shallowly downward-pointing northerly and shallowly upward-pointing southerly directions, which respectively resemble the normal and reverse detrital remanent magnetizations extracted from the Tinau Khola south

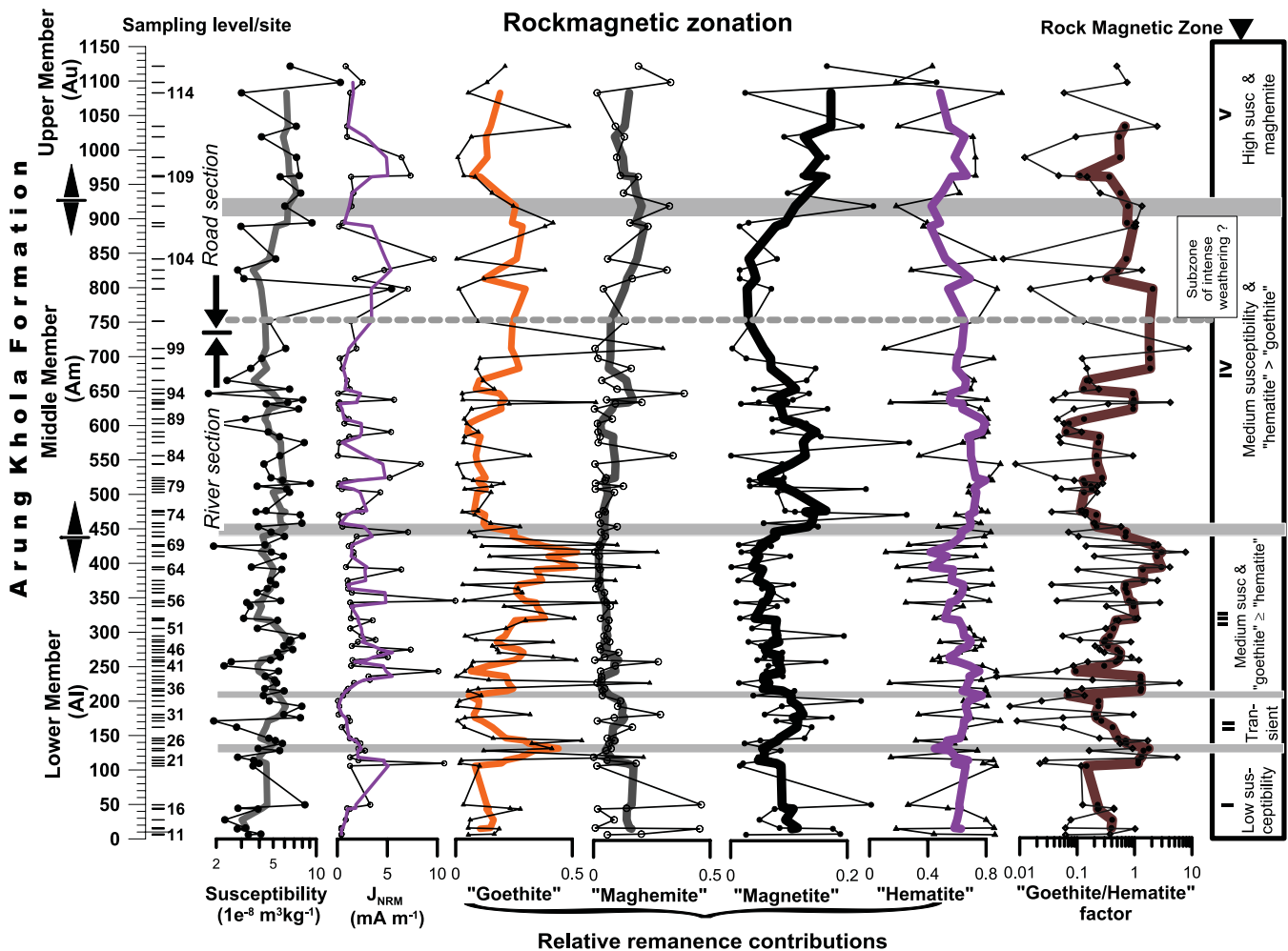


Figure 5. Logs of mass-specific MS, NRM and first-order estimates of the contributions of various minerals to the total magnetic remanence. The first-order estimates for contributions by 'goethite', 'maghemite', 'magnetite' and 'hematite' correspond to the fractional contributions of $J_{\text{NRM}} - J(150^\circ\text{C})$, $J(150^\circ\text{C}) - J(400^\circ\text{C})$, $J(400^\circ\text{C}) - J(600^\circ\text{C})$ and $J(600^\circ\text{C})$ to the total values, respectively. The 'goethite/hematite' factor is calculated as the ratio $[J_{\text{NRM}} - J(150^\circ\text{C})]/J(600^\circ\text{C})$. These data indicate a classification of five rockmagnetic zones.

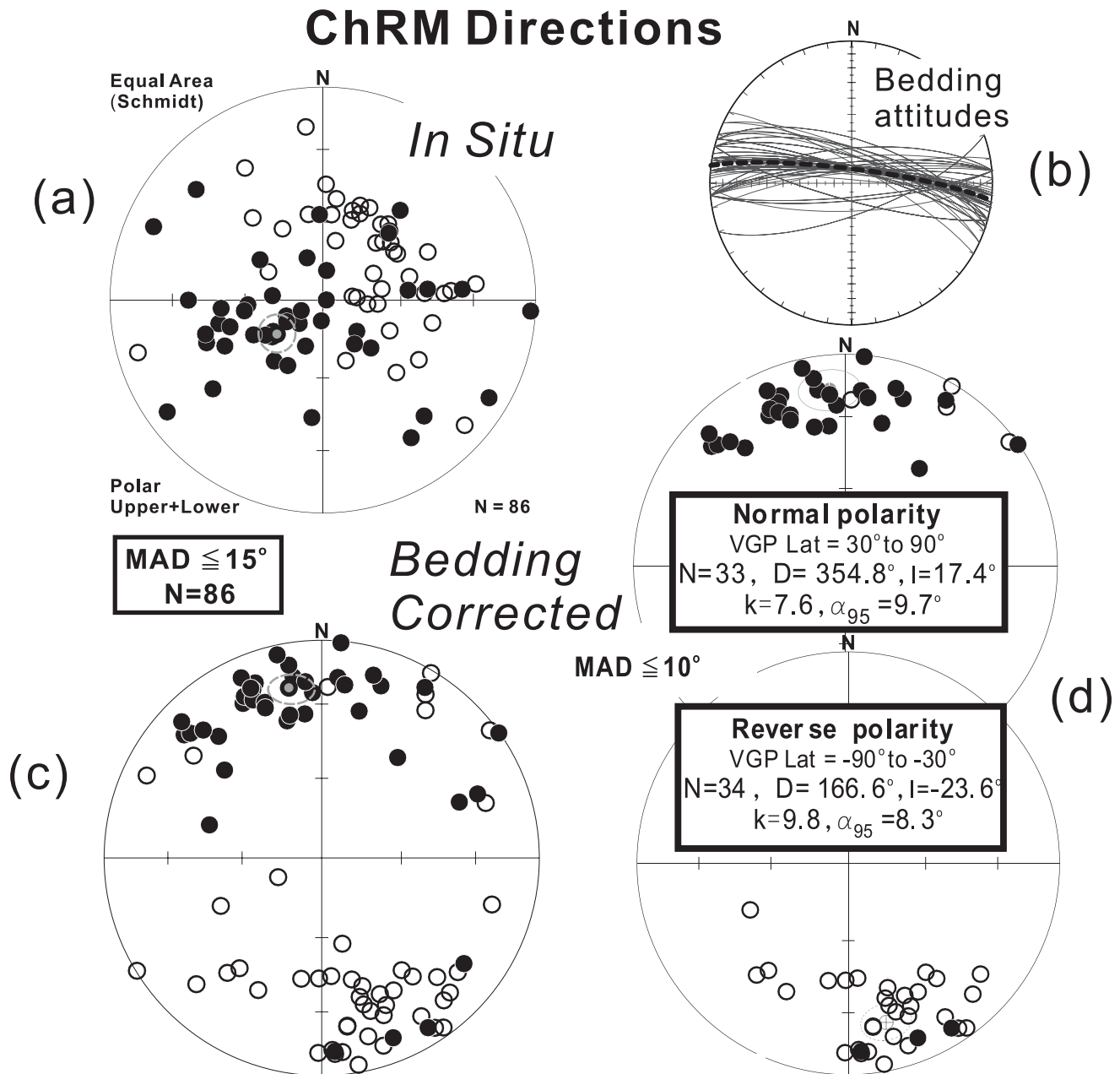
and other Nepalese Siwaliks sections (Gautam & Rösler 1999; Gautam & Fujiwara 2000). For the 86 levels, the mean directions and statistical parameters for the combined data after inversion were as follows: $D = 233.6^\circ$, $I = 68.2^\circ$, $k_b = 5.2$, $\alpha_{95} = 7.4^\circ$ (before bedding-tilt correction); $D = 348.9^\circ$, $I = 22.5^\circ$, $k_a = 5.5^\circ$, $k = 9.8$, $\alpha_{95} = 8.3^\circ$ (after bedding-tilt correction). The bedding attitudes along the Tinau-N section were subvertical (Fig. 6b) and exhibited a much smaller dispersion ($k = 43.1$ and $\alpha_{95} = 2.4^\circ$) than the mean magnetization direction before bedding correction, implying that the fold test was not applicable. However, the mixed group of steep and oppositely directed pre-tilting ChRM directions converged into two roughly antipodal populations (Fig. 6d) after tilt correction, and the overall mean direction ($D = 348.9^\circ$, $I = 22.5^\circ$) was similar to the primary detrital remanence from other Siwalik sections (Gautam 2008).

Polarity determination of the Siwalik sediments was problematic because of significant inclination shallowing recorded by the primary detrital remanence, causing inclinations too shallow to judge the polarity, especially when there was noise that led to significant departures of the declinations from north or south. Also, samples from stratigraphic levels close to reversal boundaries had intermediate ChRMs, which may lead to ambiguous polarity assignment

(Rösler & Appel 1998). Hence, we based polarity determination on the sign and value of the latitude of the calculated virtual geomagnetic pole (VGP) (normal, 90° to 30° ; reverse, -30° to -90° ; indeterminate, from -30° to $+30^\circ$), following the practice of Gautam & Fujiwara (2000). These criteria led to rejection of nine sites having indeterminate polarity. Mean directions and statistics for the remaining 77 sites were $N = 35$, $D = 349.2^\circ$, $I = 25.3^\circ$, $k = 4.1$, $\alpha_{95} = 13.8^\circ$ (normal), and $N = 42$, $D = 160.3^\circ$, $I = -34.2^\circ$, $k = 3.7$, $\alpha_{95} = 13.5^\circ$ (reverse). With a k -ratio = 1.1, observed angular difference = 11.8° , and critical angular difference = 19.2° , these data imply a positive reversal test classified as C (McFadden & McElhinny 1990). Hence, we interpreted the observed ChRM as the primary remanence.

Magnetic polarity stratigraphy

Fig. 7 shows the plots of ChRMs from 86 levels, the VGP latitude plot used to discern the polarity and the MPS for the Tinau-N section. The MPS comprises nine normal- and eight reverse-polarity zones ($N1, R1, \dots, R8, N9$) labelled from bottom to top. We identified a magnetic polarity zone as of distinct polarity, that is, normal or



Overall mean: N = 86, D = 348.9° , I = 22.54° , k = 5.5, $\alpha_{95} = 7.2^\circ$

Best-defined mean: N = 67, D = 351.8° , I = 20.9° , k = 7.8, $\alpha_{95} = 6.6^\circ$

Figure 6. Summary of characteristic remanence (ChRM) directions from the Tinau Khola north section (Tinau-N; Siwalik Group, North Belt). In the stereographic projections, each symbol represents a direction (solid, downward; open, upward) obtained from single core specimen at a distinct stratigraphic level. For the combined ChRMs or each polarity cluster, the Fisherian mean directions are shown with respective confidence ellipses at the 95 per cent probability level. (a) *In situ* ChRMs calculated from demagnetization data points mostly above 600°C from 86 levels satisfying the criterion of maximum angular deviation (MAD) $\leq 15^\circ$ before bedding-tilt correction. These directions obviously differ from the RF estimates or the present-day dipole field direction ($I = 47^\circ$). (b) Subvertical (northerly dips, normal; southerly dips, overturned) bedding planes measured in the field and used for bedding-tilt correction. Limited dispersion in bedding attitudes prohibited use of the fold test. (c) Bedding-tilt corrected ChRMs from 86 levels that roughly converged into two antipodal clusters. Assignment of polarity was ambiguous for several directions with intermediate positions. (d) ChRM directions satisfying MAD $\leq 10^\circ$ and having an unambiguous polarity assignment (normal, VGP latitude $\leq -30^\circ$; reverse, VGP $\geq 30^\circ$), used for calculating the best-defined mean for the Tinau-N section.

reverse (excluding indeterminate), even if it was supported only by a single sampling level. For age assignment, we correlated the MPS with the global polarity timescale (GPTS) proposed by Lourens *et al.* (2004).

Absolute age data constraining the depositional ages of geological formations are not available for the Nepalese Siwaliks, and the fossils found so far do not permit assigning age even with an accuracy of *ca.* 1 Myr. Therefore, correlations must be based on

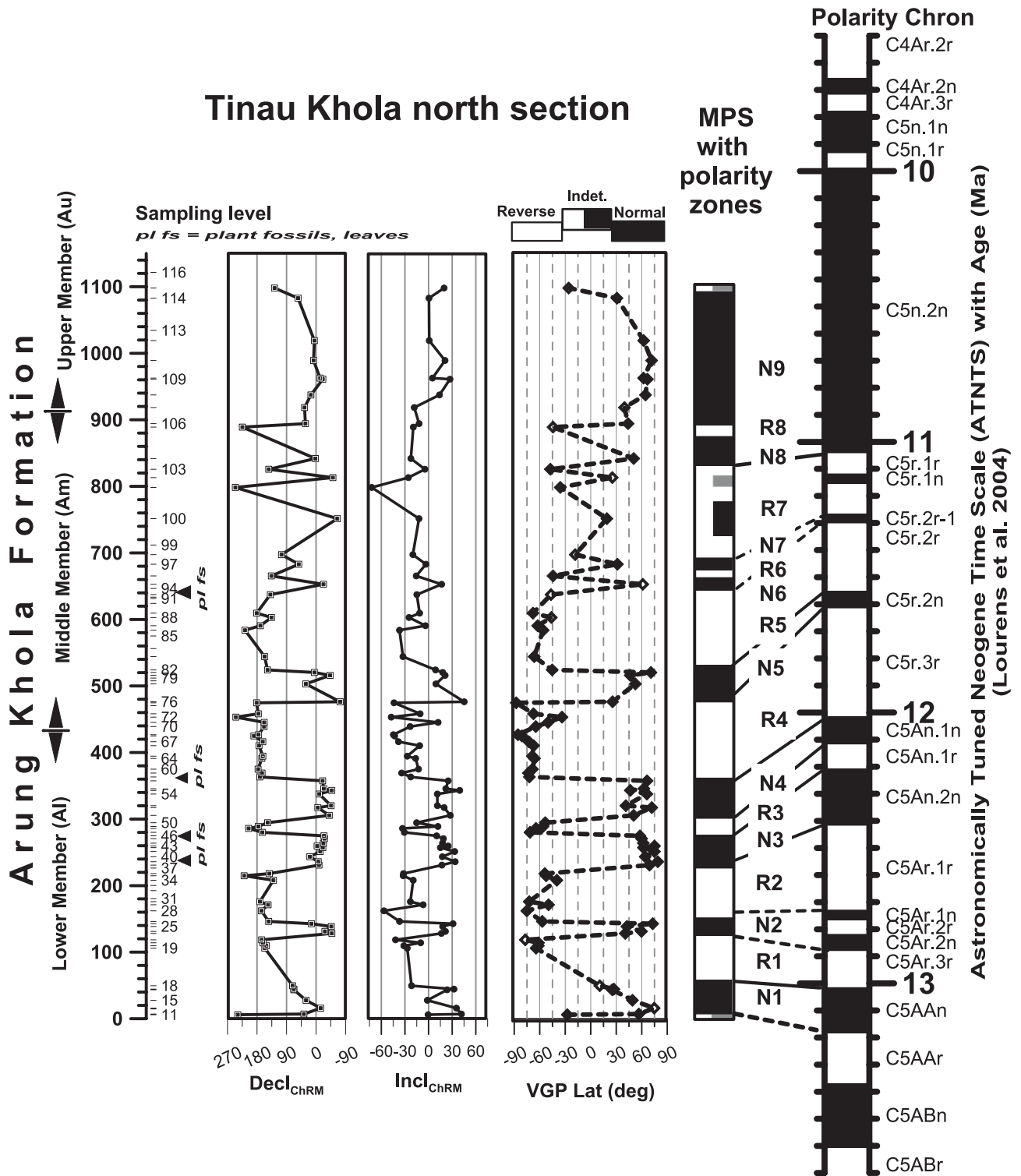


Figure 7. Logs of declinations ($Decl_{ChRM}$) and inclinations ($Incl_{ChRM}$) of the characteristic remanence and virtual geomagnetic pole latitudes (VGP Lat). For the latitude data, solid and open diamonds denote values for ChRM directions having a maximum angular deviation ($MAD \leq 10^\circ$), and $10^\circ < MAD \leq 15^\circ$, respectively. We distinguished nine normal ($N1-N9$) and eight reverse ($R1-R8$) polarity zones and used them to construct the Tinau-N magnetic polarity sequence (MPS), which we then correlated with the standard polarity timescale shown at the right to assign depositional ages. The base of the Tinau-N section is at ca. 13.2 Ma, whereas its topmost part falls within Chron C5n.2n, dated at 9.987–11.040 Ma.

previous magnetostratigraphic results constraining the ages of formational or subdivisional boundaries. Published chronological data provide some constraints on the age limits for the Arung Khola Upper (Au) and Middle (Am) members. Au is located above 918 m

in the present section and is marked by the appearance of ‘salt and pepper’ type sandstones; at the base it exhibits lithofacies comprising a higher proportion of sandstones over the rarely variegated mudstones. It differs considerably from Am, in which frequently

variegated mudstones and fine sandstones occur in almost equal amounts. The top of Au is constrained in the Tinau-S section, where it is very close to the hominoid fossil (*Sivapithecus punjabicus*) site correlated to the base of Chron C4Ar.1n (9.409 Ma), whereas the base of Au is determined from the Arung Khola–Murali Khola (AM) section within the lower part of Chron C5n.2n (9.987–11.040 Ma), implying that it is at least older than *ca.* 10.5 Ma (Munthe *et al.* 1983; Tokuoka *et al.* 1986; Gautam & Rösler 1999). The Au/Am boundary is correlatable from magnetic polarity dating with the boundary of the Middle and Upper members of the Rapti Formation in the Bakiya Khola section, which lies within Chron C5n.2n (Harrison *et al.* 1993; Nakayama & Ulak 1999; Gautam & Rösler 1999). The base of the Tinau-N section is truncated by thrust. Moreover, the measured thickness of 918 m for Am and Al combined is much less than the *ca.* 1500 m for the same in the AM section. Because the base of the AM section dated by Tokuoka *et al.* (1986) can be related to Chron C5ACn (13.734–14.095), the maximum expected age of the Tinau-N section is significantly lower than *ca.* 14.1 Ma.

Following the above reasoning, we interpret the uppermost 264-m interval with predominantly normal polarity (*N8* and *N9*) to belong to Chron C5n.2n (Fig. 7). We ignore Chron R8 as a possible cryptochron within Chron C5n.2n. Further matching of the patterns in the MPS with the GPTS leads to correlation of alternating polarity zones *N5* to *R2* with the successive polarity chrons from C5r.2n to C5r.1r, and *N1* with C5AAN. We consider correlations for the remaining zones to be tentative and show them with dotted lines in Fig. 7. Polarity zone *R7* is poorly defined, owing partly to a scarcity of drillable sites around level 100. The proposed correlation implies a most plausible age of *ca.* 13.2 Ma (Chron C5AAN: 13.015–13.183 Ma) for the base, and an estimated age of the topmost part somewhere close to the middle of Chron C5n.2n (9.987–11.040 Ma).

From the magnetostratigraphic correlation suggested here, the exposed base of the Arung Khola Lower Member in Tinau-N extends down to at least *ca.* 13.2 Ma, and deposition of the 1100-m thick section spanned *ca.* 2.7 Myr. In a review of magnetostratigraphic data from the Arung Khola–Tinau Khola area, Gautam & Rösler (1999) reestimated the age spans of the AM and Tinau-S (TK) sections to be 14–7 Ma, and 11.4–6 Ma, respectively, whereas they placed the lower–middle (Al–Am) and middle–upper (Am–Au) boundaries of the Arung Khola Formation at 12.5 Ma and 10.5 Ma, respectively. From this study, the revised age estimate for the Al–Am boundary marked by the beginning of the predominance of hematite over goethite, shown by a drastic decrease in the ‘goethite/hematite’ factor, is *ca.* 11.8 Ma. The Am–Au boundary, which corresponds to the marked increase in susceptibility and the contribution of soft-coercivity minerals, inferred to be magnetite and maghemite, also falls within long, normal-polarity Chron C5n.2n (9.987–11.040), but close to its lower age limit.

Konomatsu (1997) studied plant-fossil leaves from the Arung Khola and Binai Khola Formations in the Tinau Khola area. Plant leaves from one site each in Al and Am in the Tinau-N section (within sampling levels 18–25 and 70–75, respectively; see Fig. 7) represent tropical rain forest elements (*Ziziphus*, *Gynocardia*, *Orophea*, *Bambusa*, *Cynametra*, etc.) but clearly lack tall trees such as *Dipterocarpus*. These assemblages were categorized as the CP-1 zone. However, two sites from Au in the Tinau-S section yielded assemblages dominated by tropical wet evergreen elements (*Dipterocarpus*, *Shorea*, *Hopea*, *Calophyllum*, etc.) related to the CP-2 zone. According to Konomatsu (1997), the upper part of Au may be correlated to the *Dipterocarpus*-bearing beds of the Chor Khola Formation (in the Surai Khola section) dated magnetically at

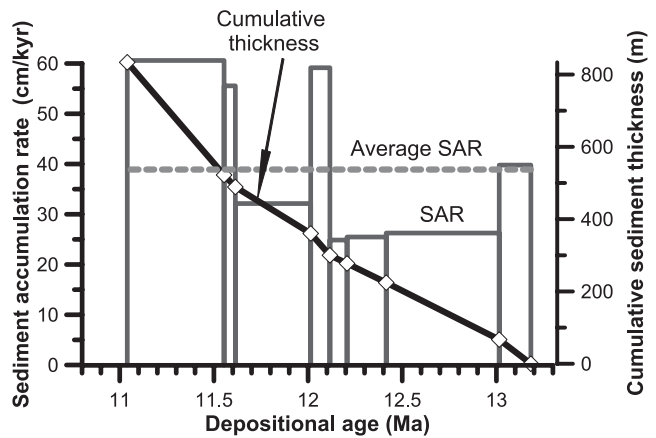


Figure 8. Plots of sediment accumulation rates (SARs) and cumulative thickness for the Tinau-N section. A low SAR (25 cm kyr^{-1}) below *ca.* 12.1 Ma followed by an increasing trend that leads to maximum values 11.5–11.0 Ma.

11.4–8.3 Ma (Appel *et al.* 1991; recalibration by Gautam & Rösler 1999). These inferences from plant fossil data are consistent with our proposed correspondence of the top of the magnetostratigraphically dated Tinau-N section (i.e. the lower part of Au) to the middle of Chron C5n.2n.

Sediment accumulation rate

Because of the incompleteness of the uppermost part of the measured section related to long polarity Chron C5n.2n, we limited estimation of the SAR to the stratigraphic interval comprising the lower 834 m. For the 2.14 Myr spanned by the MPS below Chron C5n.2n, the average SAR estimate was 38.9 cm kyr^{-1} , which considerably exceeded the 29.6 cm kyr^{-1} value newly estimated for the Karnali section over the same duration. SAR ranged from 24.9 to 60.6 cm kyr^{-1} for chronologically well-constrained intervals (Fig. 8). It was mostly 25 cm kyr^{-1} before *ca.* 12.1 Ma, after which there was an increasing trend leading to the highest value during *ca.* 11.5–11 Ma. These estimates are reasonable, judging from average values of 31.7 – 49.6 cm kyr^{-1} obtained for nine sections throughout Nepal (Gautam & Fujiwara 2000). However, the increase in SAR after *ca.* 12.1 Ma (above 300 m) needs further study in regard to its probable relationship to an earlier phase of uplift and intense unroofing of the main Himalayan region that served as the sediment source, subsequent accumulation of sediments in the Siwalik foredeep and the role of the monsoonal climate during that time.

Magnitudes of tectonic rotation and inclination shallowing

We estimated the magnitude and sense of relative rotation about the vertical of the Tinau-N belt, and the amount of inclination flattening as the combined effect of (i) the southerly location of the study area on a part of the Indian Plate moving northward, and (ii) inclination shallowing related to the detrital remanence residing in specular hematite. For this purpose, we used the observed mean primary remanence corrected for bedding tilt ($D_{\text{obs}} = 351.8^\circ$, $I_{\text{obs}} = 20.9^\circ$, $k = 7.8$, $\alpha_{95} = 6.6^\circ$), calculated from 67 ChRM directions combined that satisfied the criteria of $\text{MAD} \leq 10^\circ$ and distinct polarity (i.e. VGP latitudes outside -30° – 30°). To derive the rotation and flattening parameters (Table 2), we compared the estimate with the expected directions (D_{exp} , I_{exp}) by using two apparent polar wander paths

Table 2. Estimation of magnitudes of rotation and flattening derived from the observed primary remanence (ChRM) in the Tinau-N section (27.75°N, 83.51°E).

Estimated North Pole position			Declination data			Rotation	Inclination data			Flattening (inclination shallowing)		
APWP source	Age	PLAT	PLONG	D_{exp}	dDx	D_{obs}	$R \pm dR$	I_{exp}	dIx	I_{obs}	$F \pm dF$	f
Klootwijk <i>et al.</i> (1985)	10 Ma	83.1	303.2	-4.8	3.2	-8.2	-3.4 ± 6.2	39.4	4.2	20.9	18.5 ± 6.3	0.46
Acton (1999)	10–13 Ma	88.9	215.0	1.0	5.3	-8.2	-9.2 ± 7.1	45.5	3.7	20.9	24.5 ± 6.1	0.38

Note: For APWP data after Klootwijk *et al.* (1985) and Acton (1999), A_{95} uncertainties are 3° and 4.7°, respectively. Expected directions (D_{exp} , I_{exp}), their error limits (dDx , dIx), rotation and flattening (R , F) magnitudes and associated errors (dR , dF) as well as the factor f were calculated following the expressions given in Butler (1992).

for India, here termed APWP_K (after Klootwijk *et al.* 1985) and APWP_A (after Acton 1999). Using APWP_K suggests a significantly southward location for the present Tinau-N area during the time of remanence acquisition, consistent with an I_{exp} of 39.4°, whereas the difference $I_{\text{exp}} - I_{\text{obs}} = 18.5^\circ$ accounts for inclination flattening. The latter is the effect of inclination shallowing, according to $f = \tan(I_{\text{obs}})/\tan(I_{\text{exp}}) = 0.46$. On the other hand, use of APWP_A results in a negligible northward motion of India during the last 10 Myr, such that the expected inclination would be 45.5° (i.e. closer to the dipole field direction of $I = 47^\circ$). This requires a stronger inclination shallowing ($f = 0.38$) to explain the flattening of inclination by 24.5°. The estimated values of f and the inclination differences are consistent with experimental and field data related to detrital remanent magnetization recorded by oblate hematite grains (Tauxe & Kent 1984; Butler 1992). Use of APWP_K suggests that the Tinau-N belt has been rotated by 3.4° anticlockwise about the vertical axis with respect to a stable India since the time of remanence acquisition at 10 Ma. In contrast, APWP_A implies a larger amount (9.2°) of anticlockwise rotation.

Relative rotation among the North and South belts along the CCT

The best estimates of mean primary remanence from two sections along the Tinau Khola River separated by the CCT ($N1 = 77$, $D1 = 343.1^\circ$, $I1 = 22.2^\circ$, $R1 = 72.4$, $k1 = 16.4$, $\alpha_{195} = 4.1^\circ$ for Tinau-S at 11.5–5.9 Ma, after Gautam (2008); $N2 = 67$, $D2 = 351.8^\circ$, $I2 = 20.9^\circ$, $R2 = 58.5$, $k2 = 7.8$, $\alpha_{295} = 6.6^\circ$ for Tinau-N at ca. 13.2–10.5, shown in Fig. 6d, this study) can be used to test for differential rotation among the two belts (Fig. 1). Based on calculations in Table 2, the difference in expected remanence direction between these two localities may be practically ignored for comparison, owing to their age spans and coordinates. With an angular difference of 8.2° between these two estimates, their α_{95} confidence regions show slight overlap. However, as the α_{95} confidence region of one set does not include the mean of the other set, the similarity of these estimates can neither be accepted nor refuted at 95 per cent probability level. To solve this, we applied Watson's F test outlined in Butler (1992), as follows:

$$N = N1 + N2 = 144; R \text{ (resultant of } N \text{ unit vectors)} = 130.6;$$

$$F_{\text{obs}} = (N - 2) * (R1 + R2 - R) / (N - R1 - R2) = 3.14;$$

$$\text{Tabulated } F\text{-statistic } F_{\text{tab}}(2, 2 * (N - 2)) = F_{\text{tab}}(2, 284) = 3.03.$$

From $F_{\text{tab}} < F_{\text{obs}}$, these mean directions from Tinau-S and Tinau-N can be considered to be different at the 5 per cent significance level. These two means and related uncertainties yield $R \pm dR = -8.7^\circ \pm 6.7^\circ$, suggesting that the South Belt has undergone an anticlockwise rotation of about 9° (with a possible range

of 15°–2°) with respect to the North Belt. Such rotation estimates need further investigation to understand their implications for the nature and extent of rotational underthrusting along the CCT, which is prominent throughout the Nepalese sub-Himalaya (Tokuoka *et al.* 1986).

Low-field MS and its anisotropy

The magnetic fabrics of several Siwalik sections have been studied based on measurements to determine the principal AMS directions ($\kappa_{\text{max}} \geq \kappa_{\text{int}} \geq \kappa_{\text{min}}$), and the shape factor (T) and corrected degree of anisotropy (P') have been calculated to understand the quality and quantity of the fabrics, respectively. We made calculations using the following expressions from Jelinek (1981):

$$T = (2\eta_{\text{int}} - \eta_{\text{max}} - \eta_{\text{min}}) / (\eta_{\text{max}} - \eta_{\text{min}}),$$

$$P' = \exp \sqrt{2 [(\eta_{\text{max}} - \eta_m)^2 + (\eta_{\text{int}} - \eta_m)^2 + (\eta_{\text{min}} - \eta_m)^2]},$$

where

$$\eta_{\text{max}} = \ln \kappa_{\text{max}}; \eta_{\text{int}} = \ln \kappa_{\text{int}}; \eta_{\text{min}} = \ln \kappa_{\text{min}}; \eta_m = \ln \kappa_m,$$

and

$$\kappa_m = (\kappa_{\text{max}} + \kappa_{\text{int}} + \kappa_{\text{min}}) / 3 \text{ is the mean susceptibility.}$$

On the scale of a site or section, clustered κ_{min} axes correspond to the pole of the 'magnetic foliation plane', whereas clustered κ_{max} axes define the 'magnetic lineation'. The condition $0 < T \leq 1$ indicates oblate ellipsoid, whereas $-1 \leq T < 0$ indicates prolate ellipsoid.

Fig. 9 shows variation in MS and AMS parameters (P' and T) with stratigraphic height along the Tinau-N section. Bulk MS (κ_m) magnitudes for single specimens at distinct stratigraphic levels were commonly lower than $<10^{-7} \text{ m}^3 \text{ kg}^{-1}$ indicating a contribution from primarily paramagnetic and diamagnetic minerals (Rochette *et al.* 1992). The magnetic fabric was represented by mainly oblate susceptibility ellipsoids with a low degree of anisotropy ($P'_{\text{max}} = 1.16$). There was a distinct susceptibility increase just above the Am/Au boundary. The degree of anisotropy (P') was comparatively low and stable below level 100, after which it exhibited frequent oscillations. In view of the coincidence of this boundary (99–100) with the change from the river to the road section, P' enhancement may partially have been an artefact of increased weathering, leading to the production of iron oxides, probably maghemite. Increased bulk susceptibilities that correlated with P' were clear for the interval between 104 and 111. The shape parameter could be used to subdivide the section roughly into three zones: (i) a lower part up to level 91, characterized by predominantly oblate ellipsoids but including triaxial and slightly prolate ellipsoids; (ii) a middle part

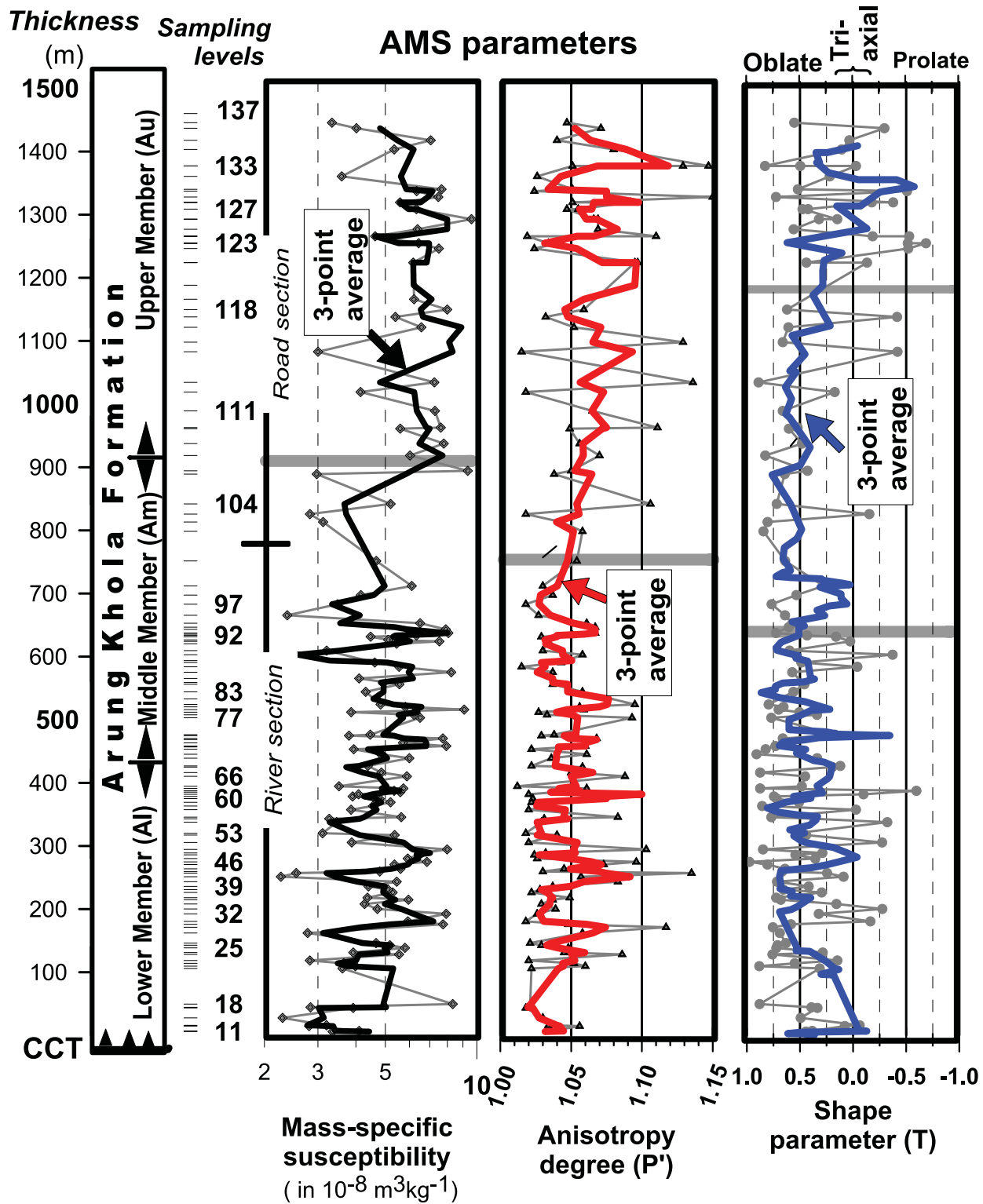


Figure 9. Logs of mean mass-specific magnetic susceptibility, Jelinek’s corrected degree of anisotropy (P'), and the shape of magnetic anisotropy ellipsoid (T) parameters, which together define the magnetic fabric intensity in the Tinau-N section. Note the marked increase in susceptibility above Am/Au boundary. A consistently low degree of anisotropy is evident throughout the river section up to level 99. The lower and upper zones discriminated by T exhibit higher variability in shape and a clear predominance of either oblate or prolate, respectively.

between levels 92 and 119, where the ellipsoids were strongly and rather consistently oblate; and (iii) an upper part above level 120, where the ellipsoids were highly variable, ranging from strongly oblate through triaxial to moderately prolate (Fig. 9, right). The

changes in shape may be partly attributed to an upward coarsening in the grain size of sediments.

Fig. 10 shows the bedding-tilt corrected AMS directions (κ_{\min} , κ_{\max}) for the whole 1450-m-thick section. The subvertical nature of

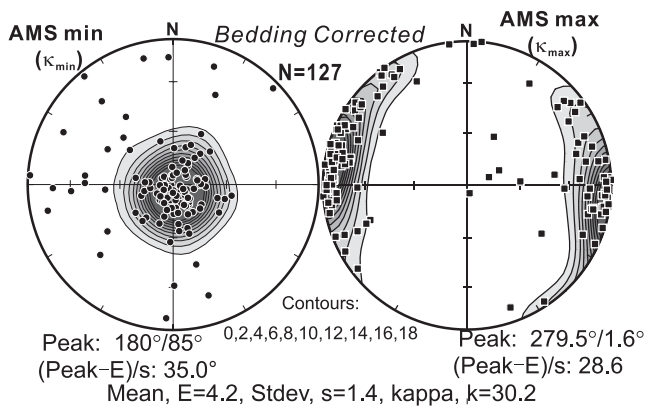


Figure 10. Stereograms (Smith equal-area projections) showing the bedding-tilt-corrected AMS minimum and maximum axes, which correspond to the magnetic foliation poles and magnetic lineations, respectively. Density contours (as multiples of sigma) and peak trend/plunge estimates were based on the Gaussian smoothing ($E = 3$ sigma) model of Robin & Jowett (1986). N , number of sites/levels, each with single specimen; Mean E , mean expected value; SD , standard deviation; k , counting function calculated as $2(1+N/9)$.

κ_{\min} (poles to magnetic foliation) indicates a planar fabric component parallel with the palaeohorizontal (bedding plane), implying a predominantly sedimentary-compactional magnetic fabric. The magnetic lineations defined by κ_{\max} were within or close to the bedding plane, that is, the palaeohorizontal plane. They were subparallel to the bedding strikes (partly illustrated in Fig. 6b) observed in the area. In analogy to earlier findings (Sagnotti *et al.* 1999; Gautam 2008 and references therein), we assumed the nearly W–E magnetic lineations to have resulted from S–N compression active during foredeep deposition, and thus to be parallel to the direction of the minimum principal horizontal stress in palaeogeographic coordinates. Comparison of the peak lineation trends obtained in this study by density modelling with the Gaussian smoothing function (Robin & Jowett 1986) for Tinau-N ($279.5^\circ/1.6^\circ$; Fig. 6) and Tinau-S (peak lineation = $267.5^\circ/4.6^\circ$ for 112 levels, detailed in Gautam (2008)) revealed a difference of 12° , which is consistent with the inference from remanence data that the South Belt has undergone an anticlockwise rotation of $ca. 9^\circ \pm 7^\circ$ with respect to the North Belt in the Tinau Khola area.

CONCLUSIONS

The magnetic polarity record based on primary depositional remanence for the *ca.* 1120-m-thick Tinau-N section suggests a depositional age of 13.2–*ca.* 10.5 Ma. The part more than 11 Ma in age yielded an average SAR of 38.9 cm kyr^{-1} . The magnetic fabric determined for a 1450-m-thick section is a composite of primary sedimentary-compactional foliation and secondary tectonic WNW–ESE directed lineation inferred to be orthogonal to the direction of tectonic convergence in the area, as found in many other parts of the Nepalese sub-Himalaya where the FBS were deposited in a syn-tectonic compressive setting. Comparison of the primary remanence data from the Tinau Khola north and south sections points to *ca.* $9^\circ \pm 7^\circ$ of rotation of the sub-Himalayan South Belt relative to the North Belt in the study area. A difference of 12° among the peak magnetic lineation estimates also supports this inference.

We found the base of the Tinau-N section to be 1.7 Myr older than that of Tinau-S, estimated at *ca.* 11.5 Ma. As these are the most easily accessible sections in the Nepalese sub-Himalaya, our

additional archive of dated sediments in Tinau-N will surely attract cross-disciplinary research teams interested in determining palaeoenvironmental and climatic proxies essential for understanding the tectonic history and the evolution of the monsoon climate in the Himalayan region.

ACKNOWLEDGMENTS

This research was funded by a MEXT/JSPS Grant-in-Aid for Scientific Research to PG (*kiban kenkyū* C, No. 17540427). We thank E. Appel (University of Tübingen) and K. Kodama (Kochi Core Centre, Kochi University) for use of their laboratory facilities; M.H. Dick for editing the English; and A. Rapalini, an anonymous reviewer, and A. Biggin (Editor) for detailed and constructive suggestions on the manuscript.

REFERENCES

- Acton, G.D., 1999. Apparent polar wander of India since the Cretaceous with implications for regional tectonics and true polar wander, *Mem. Geol. Soc. India*, **44**, 129–175.
- Appel, E., Rösler, W. & Corvinus, G., 1991. Magnetostratigraphy of the Miocene-Pleistocene Surai Khola Siwaliks in west Nepal, *Geophys. J. Int.*, **105**, 191–198.
- Beek van der, P., Xavier, R., Mugnier, J.-L., Bernet, M., Huyghe, P. & Labrin, E., 2006. Late Miocene–Recent exhumation of the central Himalaya and recycling in the foreland basin assessed by apatite fission-track thermochronology of Siwalik sediments, Nepal, *Basin Res.*, **18**(4), 413–434.
- Bernet, M., Beek van der, P., Pik, R., Huyghe, P., Mugnier, J.-L., Labrin, E. & Szulc, A., 2006. Miocene to Recent exhumation of the central Himalaya determined from combined detrital zircon fission-track and U/Pb analysis of Siwalik sediments, western Nepal, *Basin Res.*, **18**(4), 393–412.
- Burbank, D.W., Beck, R.A. & Mulder, T., 1996. The Himalayan foreland basin, in *The Tectonic Evolution of Asia*, pp. 149–188, eds Yin, A. & Harrison, M., Cambridge University Press, Cambridge.
- Butler, R.F., 1992. *Paleomagnetism: Magnetic Domains to Geologic Terranes*, Blackwell Scientific, Boston, MA, 319pp.
- Cande, S.C. & Kent, D.V., 1995. Revised calibration of the geomagnetic polarity timescale for the Late Cretaceous and Cenozoic, *J. geophys. Res.*, **100**, 6093–6095.
- Dhital, M.R., Gajurel, A.P., Pathak, D., Paudel, L.P. & Kizaki, K., 1995. Geology and structure of the Siwaliks and Lesser Himalaya in Surai Khola-Bardanda area, Mid Western Nepal, *Bull. Dept. Geol., Tribhuvan Univ., Nepal*, **4**, 1–70.
- Dunlop, D.J. & Özdemir, Özden 1997. *Rock Magnetism: Fundamentals and Frontiers*, Cambridge University Press, Cambridge, 573pp.
- Flynn, L.J., Pilbeam, D., Jacobs, L.L., Barry, J.C., Behrensmeier, A.K. & Kappelman, J.W., 1990. The Siwaliks of Pakistan: time and faunas in a Miocene terrestrial setting, *J. Geol.*, **98**, 589–604.
- Friedman, R., Gee, J., Tauxe, L., Downing, K. & Lindsay, E., 1992. The magnetostratigraphy of the Chitarwata and lower Vihowa formations of the dera Ghazi Khan area, Pakistan, *Sediment. Geol.*, **81**, 253–268.
- Gautam, P., 2008. Magnetic fabric of the Siwalik sediments (Nepal): implications to the time-space evolution of the stress field, *J. Nepal Geol. Soc.*, **38**, 39–48.
- Gautam, P. & Appel, E., 1994. Magnetic-polarity stratigraphy of Siwalik Group sediments of Tinau Khola section in west central Nepal, revisited, *Geophys. J. Int.*, **117**, 223–234.
- Gautam, P., Blaha, U. & Appel, E., 2005a. Integration of magnetism and heavy metal chemistry of soils to quantify the environmental pollution in Kathmandu, Nepal, *Island Arc*, **14**(4), 424–435.
- Gautam, P., Blaha, U. & Appel, E., 2005b. Magnetic susceptibility of dust-loaded leaves as a proxy of traffic related heavy metal pollution in Kathmandu city, Nepal, *Atmos. Environ.*, **39**, 2201–2211.

- Gautam, P. & Fujiwara, Y., 2000. Magnetic polarity stratigraphy of Siwalik Group sediments of Karnali River section in western Nepal, *Geophys. J. Int.*, **142**, 812–824.
- Gautam, P., Hosoi, A., Regmi, K.R., Khadka, D.R. & Fujiwara, Y., 2000. Magnetic minerals and magnetic properties of the Siwalik Group Sediments of the Karnali river section in Nepal, *Earth Planets Space*, **52**, 337–345.
- Gautam, P. & Rösler, W., 1999. Depositional chronology and fabric of Siwalik Group sediments in central Nepal from magnetostratigraphy and magnetic anisotropy, *J. Asian Earth Sci.*, **17**, 659–682.
- Harrison, T.M., Copeland, P., Hall, S.A., Quade, J., Burner, S., Ojha, T.P. & Kidd, W.S.F., 1993. Isotopic preservation of Himalayan/Tibetan uplift, denudation, and climatic histories in two molasse deposits, *J. Geol.*, **101**, 157–175.
- Huyghe, P., Mugnier, J.L., Gajurel, A.P. & Delcaillau, B., 2005. Tectonic and climatic control of the changes in the sedimentary record of the Karnali River section (Siwaliks of western Nepal), *Island Arc*, **14**(4), 311–327.
- Jelinek, V., 1981. Characterization of magnetic fabric of rocks, *Tectonophysics*, **79**, T63–T67.
- Kirschvink, J.L., 1980. The least-squares line and plane and the analysis of palaeomagnetic data, *Geophys. J. R. astr. Soc.*, **62**, 699–718.
- Klootwijk, C.T., Conaghan, P.J. & Powell, C. McA., 1985. The Himalayan Arc: large-scale continental subduction, oroclinal bending and back-arc spreading, *Earth planet. Sci. Lett.*, **75**, 167–183.
- Konomatsu, M., 1997. Miocene leaf-fossil assemblages of the Churia (Siwalik) Group in Nepal and their paleoclimatic implication, *J. Geol. Soc. Japan*, **103**(3), 265–274.
- Kruiver, P.K., Dekkers, M.J. & Heslop, D., 2001. Quantification of magnetic coercivity components by the analysis of acquisition curves of isothermal remanent magnetization, *Earth planet. Sci. Lett.*, **189**, 269–276.
- Lee, T.Q., Kissel, C., Laj, C., Horng, C.S. & Lue, Y.T., 1990. Magnetic fabric analysis of the Plio-Pleistocene sedimentary formations of the Coastal Range of Taiwan, *Earth planet. Sci. Lett.*, **98**, 23–32.
- Lourens, L., Hilgen, F.J., Shackleton, N.J., Laskar, J. & Wilson, D., 2004. The Neogene Period, in *A Geological Time Scale 2004*, pp. 409–440, eds Gradstein, F.M., Ogg, J.G., Smith, A.G., Cambridge University Press, Cambridge.
- McFadden, P.L. & McElhinny, M.W., 1990. Classification of the reversal test in palaeomagnetism, *Geophys. J. Int.*, **103**, 725–729.
- Molnar, P., 2005. Mio-Pliocene growth of the Tibetan Plateau and evolution of East Asian Climate, *Palaeontologia Electronica*, **8**(1), 2A, 23.
- Mugnier, J.L., Mascle, G. & Faucher, T., 1993. Structure of the Siwaliks of western Nepal: an intracontinental accretionary prism, *Int. Geol. Rev.*, **35**, 1–16.
- Munthe, J., Dangol, B., Hutchison, J.H., Kean, W.F., Munthe, K. & West, R.M., 1983. New fossil discoveries from the Miocene of Nepal include a hominoid, *Nature*, **303**, 331–333.
- Nakayama, K. & Ulak, P.D., 1999. Evolution of fluvial style in the Siwalik Group in the foothills of the Nepal Himalaya, *Sediment. Geol.*, **125**, 205–224.
- Ojha, T.P., Butler, R.F., Quade, J., DeCelles, P.G., Richards, D. & Upreti, B.N., 2000. Magnetic polarity stratigraphy of the Neogene Siwalik Group at Khutia Khola, Farwestern Nepal, *Geol. Soc. Am. Bull.*, **112**, 424–434.
- Opdyke, N.D., 1990. Magnetic stratigraphy of Cenozoic terrestrial sediments and mammalian dispersal, *J. Geol.*, **98**, 621–637.
- Peters, C. & Dekkers, M.J., 2003. Selected room temperature magnetic parameters as a function of mineralogy, concentration and grain size, *Phys. Chem. Earth*, **28**, 659–667.
- Robin, P.-Y.F. & Jowett, E.C., 1986. Computerized density contouring and statistical evaluation of orientation data using counting circles and continuous weighting functions, *Tectonophysics*, **121**, 207–223.
- Robion P., Grelaud, S. & de Lamotte, D.F., 2007. Pre-folding magnetic fabrics in fold-and-thrust belts: why the apparent internal deformation of the sedimentary rocks from the Minervois basin (NE—Pyrenees, France) is so high compared to the Potwar basin (SW—Himalaya, Pakistan)?, *Sediment. Geol.*, **196**, 181–200.
- Rochette, P., Jackson, M. & Aubourg, C., 1992. Rock magnetism and the interpretation of anisotropy of magnetic susceptibility, *Rev. Geophys.*, **30**(3), 209–226.
- Rösler, W. & Appel, E., 1998. Fidelity and time resolution of the magnetostratigraphic record in Siwalik sediments: high-resolution study of a complete polarity transition and evidence for cryptochrons in Miocene fluvial section, *Geophys. J. Int.*, **135**, 861–875.
- Rösler, W., Metzler, W. & Appel, E., 1997. Neogene magnetic polarity stratigraphy of some fluvial Siwalik sections, Nepal, *Geophys. J. Int.*, **130**, 89–111.
- Sagnotti, L., Speranza, F., Winkler, A., Mattei, M. & Fucicello, R., 1998. Magnetic fabric of clay sediments from the external northern Apennines (Italy), *Phys. Earth planet. Inter.*, **105**, 73–93.
- Sagnotti, L. et al., 1999. Magnetic anisotropy of Plio-Pleistocene sediments from the Adriatic margin of the northern Apennines (Italy): implications for the time-space evolution of the stress field, *Tectonophysics*, **311**, 139–153.
- Szulc, A.G. et al., 2006. Tectonic evolution of the Himalaya constrained by detrital 40Ar–39Ar, Sm–Nd and petrographic data from the Siwalik foreland basin succession, SW Nepal, *Basin Res.*, **18**(4), 375–391.
- Tanaka, S., 1997. Uplift of the Himalaya and climatic change at 10 Ma—Evidence from records of carbon stable isotopes and fluvial sediments in the Churia Group, central Nepal, *J. Geol. Soc. Japan*, **103**(3), 253–264.
- Tauxe, L. & Badgley, C., 1988. Stratigraphy and remanence acquisition of a palaeomagnetic reversal in alluvial Siwalik rocks of Pakistan, *Sedimentology*, **35**, 697–715.
- Tauxe, L., Constable, C., Stokking, L. & Badgley, C., 1990. Use of anisotropy to determine the origin of characteristic remanence in the Siwalik red beds of Northern Pakistan, *J. geophys. Res.*, **95**(B4), 4391–4404.
- Tauxe, L. & Kent, D.V., 1984. Properties of a detrital remanence carried by haematite from study of modern river deposits and laboratory redeposition experiments, *Geophys. J. R. astr. Soc.*, **76**, 543–561.
- Tauxe, L., Kent, D.V. & Opdyke, N.D., 1980. Magnetic components contributing to the NRM of Middle Siwalik red beds, *Earth planet. Sci. Lett.*, **47**, 279–284.
- Tokuoka, T., Takayasu, K., Hisatomi, K., Yamasaki, H., Tanaka, S., Konomatsu, M., Sah, R.B. & Rai, S.M., 1990. Stratigraphy and geologic structures of the Churia (Siwalik) Group in the Tinau Khola-Binai Khola area, West Central Nepal, *Mem. Fac. Sci. Shimane Univ.*, **24**, 71–88.
- Tokuoka, T., Takayasu, K., Yoshida, M. & Hisatomi, K., 1986. The Churia (Siwalik) Group of the Arung Khola area, West Central Nepal, *Mem. Fac. Sci. Shimane Univ.*, **20**, 135–210.
- Ulak, P.D. & Nakayama, K., 2001. Neogene fluvial systems in the Siwalik Group along the Tinau Khola section, west-central Nepal Himalaya, *J. Nepal Geol. Soc.*, **25**, 111–122.
- West, R.M., Hutchison, S. & Munthe, J., 1991. Miocene vertebrates from the Siwalik Group, western Nepal, *J. Vertebr. Palaeontol.*, **11**(1), 108–129.